Study of the Multipactor Effect in Groove Gap Waveguide Technology

José Joaquín Vague, Irene Asensio, Ángela Coves, *Senior Member, IEEE*, Ángel A. San Blas, Marta Reglero, Ana Vidal Pantaleoni, *Member, IEEE*, David Raboso, Mariano Baquero-Escudero, *Member, IEEE*, and Vicente E. Boria, *Fellow, IEEE*

***Abstract*— This article presents a theoretical and experimental comparative study of the different multipactor threshold values obtained in the rectangular waveguide (RW) and the groove gap waveguide (GGW). To this end, the multipactor effect has been first analyzed in an RW with a recently developed theoretical model. Then, the multipactor breakdown power levels in the equivalent GGW have been predicted with an accurate electron tracking code, showing a significant increment compared with the RW case. In order to validate these results, two *E*-plane WR-90 RW transformers have been designed with a full-wave electromagnetic simulation tool. The central sections of these transformers have been implemented in RW and GGW, respectively, and their multipactor breakdown power levels have also been predicted. The two designed transformers have been fabricated in aluminum and then measured in terms of electrical response (scattering parameters) and RF multipactor effect (power threshold values). All the experimental results agree well with the set of simulated data, thus fully validating the performed study.**

***Index Terms*— Groove gap waveguide (GGW), multipactor effect, rectangular waveguide, RF breakdown, waveguide transformer.**

I. Introduction

MULTIPACTOR is a well-known and undesired high-power effect that may occur in microwave components operating under high-vacuum conditions [1], [2]. These devices are present in a wide range of different scenarios, such as satellite communication payloads, traveling-wave tubes, and klystrons, as well as particle accelerators. The multipactor effect is due to an avalanche of electrons, producing a resonant discharge inside the affected component with a large number of adverse consequences [3]. Among them, we can mention the increment of signal noise and reflected power, the generation of signal harmonics, the detuning of resonant cavities, and some other negative effects (e.g. heating of device walls, outgassing, and even physical damages in the component).

Some years ago, the first multipactor susceptibility charts were obtained for parallel-plate waveguides using analytical models [4] and empirical data [5]. More recently, the multipactor effect has been studied in a wider variety of waveguides and transmission lines, such as rectangular [6]–[8], circular [9], elliptical [10], ridge [11], and coaxial waveguides [12], [13], as well as planar microstrip lines [14].

For high-power applications, a large number of components operating in high-frequency ranges (i.e., the Ku-band and even beyond 20 GHz) are still implemented in rectangular waveguide (RW) technology. However, the emergent groove gap waveguide (GGW) technology, originally proposed in [15], is becoming a very promising alternative due to its potential advantages [16], [17]. The textured surface consisting of a "Fakir's" bed of pins provides a high-impedance boundary that allows controlling the reflection coefficient seen by the surface waves [18].

A relevant feature of the GGW technology is that perfect metallic contact between its different parts (top cover and body) is not needed [19], [20]. For this reason, it is a good candidate to replace the standard hollow RW in high-frequency components (as it was demonstrated in [21] with measured data of reassembling robustness tests). For instance, the practical realization of a V-band diplexer in GGW technology can be seen in [22]. More recently, and for Ka-band applications, an asymmetric orthomode transducer has been implemented in GGW [23], and a magic-T based on a combination of ridge and *E*-plane GGWs has been designed and manufactured [24]. A novel half-air-filled substrate integrated GGW and the corresponding transition to microstrip planar technology, covering the entire W-band frequency range, have just been proposed and experimentally validated in [25]. GGW technology has also been successfully used in the field of low-profile antennas, where artificial ground planes and surfaces have been implemented [26], [27].

Despite the growing use of GGWs in high-frequency applications, there is only a recent contribution on corona discharge breakdown in this technology [28]. This article is aimed at filling this gap, by performing theoretical and experimental studies of the multipactor breakdown effect in GGW technology and comparing the results with those for the RW counterpart.

Manuscript received November 22, 2021; revised February 2, 2022; accepted February 23, 2022. Date of publication March 18, 2022; date of current version May 5, 2022. This work was supported by the Ministerio de Ciencia e Innovación, Spanish Government, through the Subprojects C41 and C43 of the Coordinated Research and Development Project PID2019-103982RB under Grant MCIN/AEI/10.13039/501100011033. *(Corresponding author: José Joaquín Vague.)*

José Joaquín Vague, Irene Asensio, Marta Reglero, Ana Vidal Pantaleoni, Mariano Baquero-Escudero, and Vicente E. Boria are with the Departamento de Comunicaciones-ITEAM, Universitat Politècnica de València, 46022 Valencia, Spain (e-mail: jvague@dcom.upv.es; vboria@dcom.upv.es).

Ángela Coves and Ángel A. San Blas are with the Department of Communications Engineering-I3E, Universidad Miguel Hernández de Elche, 03202 Elche, Spain (e-mail: angela.coves@umh.es).

David Raboso is with the European Space Research and Technology Centre (ESTEC), European Space Agency (ESA), 2201 AZ Noordwijk, The Netherlands.

Color versions of one or more figures in this article are available at https://doi.org/10.1109/TMTT.2022.3157587.

Digital Object Identifier 10.1109/TMTT.2022.3157587

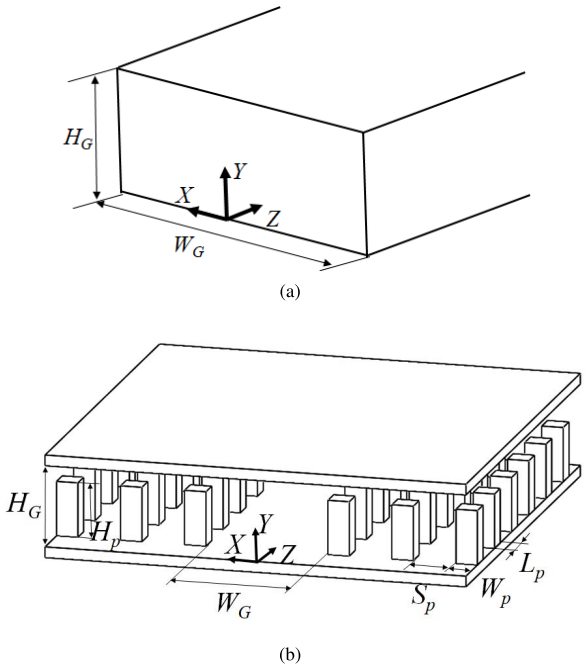

Fig. 1. Geometrical representation of the two waveguides considered in this study. (a) RW (for the standard WR-90: $W_G = 22.86$ mm and $H_G = 10.16$ mm) and (b) GGW with dimensions of $W_G = 22.86$ mm, $H_G = H_p = 10.16$ mm, $W_p = L_p = 4$ mm, and $S_p = 8$ mm.

Therefore, this article is organized as follows. First, the multipactor threshold power is theoretically analyzed in RWs with a recently developed model [29], which is successfully compared with the results of an available commercial code and a simple parallel-plate model. Then, the multipactor effect in GGW technology is studied with the cited commercial code, which is based on an electrons tracking model using the real electromagnetic fields of the GGWs. Next, in order to validate the previous theoretical comparative study, two E-plane WR-90 waveguide transformers, where the central sections are, respectively, implemented in RW and in its GGW counterpart, are designed and manufactured in aluminum. Then, the multipactor threshold levels of both transformers have been measured, showing a good agreement with the simulated data and confirming the higher threshold values of the GGW technology. Finally, the main conclusions of this work are briefly summarized.

II. Multipactor Characterization in RW and GGW

In this section, we first detail the geometries of the two considered waveguides (RW and GGW), and then, we show their multipactor threshold values using different analysis methods and software tools.

For this work, the standard WR-90 RW (with nominal values of 22.86 and 10.16 mm for its width and height, respectively) is selected, and we have focused our multipactor study in the frequency range of 10–12 GHz (upper-end side of the X-band) within the WR-90 monomode bandwidth. This frequency range is chosen according to the RF power availability in the facility where multipactor validation tests are performed, i.e., the High Power RF Space Laboratory of the European Space Agency (ESA) and the Val Space

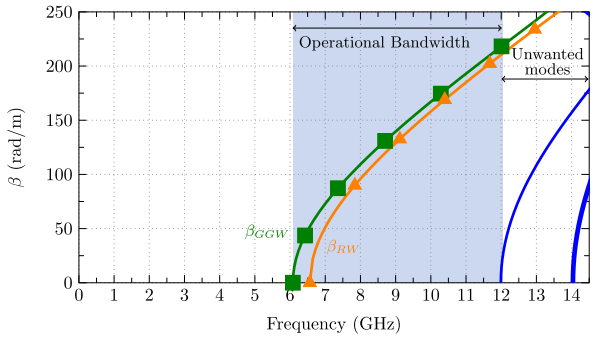

Fig. 2. Dispersion diagram of the GGW-90 (unwanted modes with solid lines and fundamental mode with square marks) and the WR-90 RW (fundamental mode with triangle marks).

TABLE I
SEY Parameters Extracted From ECSS Standard

Material	E_{max}(eV)	E_1(eV)	δ_0	δ_{max}
Aluminium	276.0	17.0	0.8	2.92

Consortium (VSC). In addition, the considered frequency range is commonly employed for transmitting the downlink channels of Ku-band satellite communications. It is important to note that the validated multipactor study can be directly scaled up to higher frequency bands, where GGW is a very promising technological solution.

The two waveguide geometries considered in this work, together with all their relevant dimensions, are shown in Fig. 1. The well-known RW is shown in Fig. 1(a), where W_G and H_G are, respectively, the width and height of the waveguide (their values for the standard WR-90 case are included in the figure caption). Fig. 1(b) displays the geometry of the GGW with all involved dimensions. It basically consists of two metal plates, where the bottom one includes a bed of pins that are periodically spaced. W_G and H_G have the same meaning for the GGW and RW (so the called GGW-90 will have the same values as its RW counterpart, in this case, the WR-90). The pins have a square cross section ($W_p = L_p$), and S_p is the separation or distance between adjacent pins. In this work, we are going to consider the zero-gap GGW (in which the height of the pins H_p is equal to H_G), as originally proposed in [30] and used in [31] to alleviate manufacturing burdens.

First, we have computed the dispersion diagram of the considered GGW-90, and the results are displayed in Fig. 2 (where solid curves correspond to unwanted modes of the GGW, and the curves with square and triangle marks are related, respectively, to the fundamental modes of the GGW and the WR-90 RW). As can be seen, the propagation behavior and the operational bandwidth of both fundamental modes are very similar, thus confirming (as has already been studied before in [17] and [32]) the equivalence of both waveguide technologies.

In addition, the magnitudes of the vertical component of the electric field (E_Y) for the fundamental mode of the two waveguides (RW and GGW) are shown in Fig. 3, where both results are normalized to the maximum value of E_Y in the RW (see dashed line). These previous results (dispersive behavior and electric field magnitude) have been computed, respectively, with the eigenmode and frequency-domain solvers of

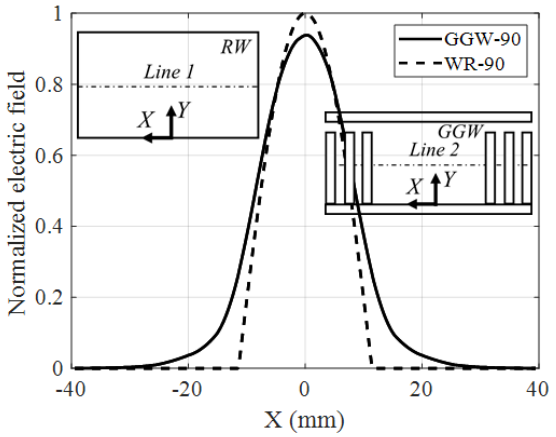

Fig. 3. Comparison of the normalized values of E_Y (computed at 11 GHz) in the RW (WR-90) and the GGW (GGW-90) along Lines 1 and 2 both located at $Y = H_G/2$.

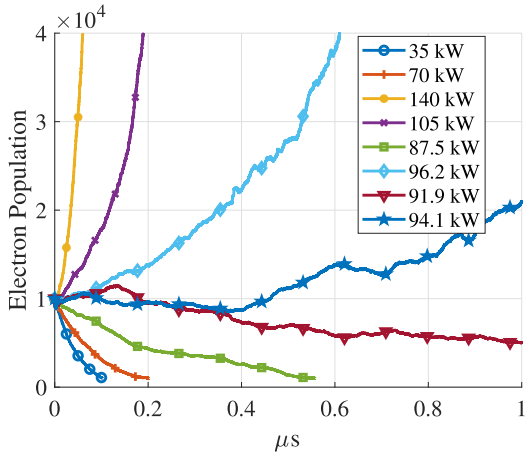

Fig. 4. Electron population evolution for the automatic power sweep computed by SPARK3D for WR-90 RW at 11 GHz.

the full-wave electromagnetic (EM) analysis tool CST Studio Suite (v.2020, Dassault Systèmes).

As can be seen in Fig. 3, the electric field in the GGW has a spread effect, having nonzero values in the bed of pins area, whereas the electric field in the RW is totally confined inside as expected. In addition, the maximum value of E_Y is reduced (around 6%) in the GGW with regard to the RW case for the same transmitted power. Since RF discharge effects are strongly dependent on the electric field distribution (and its maximum value in critical areas between metal plates), the results of Fig. 3 are a clear indication that the GGW will outperform the RW in terms of multipactor threshold levels. Let us then proceed with the corresponding comparative study.

A. Multipactor Effect in RW

Two different software tools have been used to study the multipactor effect in the RW. The first one is based on a model originally developed for dealing with partially dielectric-loaded RWs [29], which has been particularized for the standard empty RW (thus being called AIR-RW in this article).

The other employed software tool is SPARK3D (v2020, Dassault Systèmes), which first imports the EM fields inside the RW (previously computed with CST Studio Suite in this case) and then tracks the resulting electron motion by solving the 3-D Lorentz force equation. This procedure is typically used when complex structures are involved (see [33]), as it is the case of the GGW considered in Section II-B.

In order to perform all the accurate multipactor simulations included in this article with SPARK3D, the following additional consideration and configuration parameters must be taken into account.

1) The EM fields imported from CST Studio Suite must be obtained employing the available tetrahedral meshing solver, thus obtaining enough accurate information for driving the motion of electrons with a reasonable computational effort. For this purpose, an error between consecutive results (S-parameters of the considered structure) lower than 1% is fixed.
2) An initial value for the power of the microwave excitation signal in the input port of the structure under analysis must be provided (a low enough value, in the order of few tens or hundreds of W, is enough).
3) A homogeneous electron seeding must be defined inside the component under study, considering a minimum number of 10^4 electrons. In addition, as a practical criterion for multipactor event detection, a value of 100 is chosen for the growing factor of the electron population.

After SPARK3D is properly configured, the code performs an automatic power sweep to find the multipactor threshold power level for the considered structure, providing also additional output results with more information (such as the multipactor order related to the detected discharge [1] and the evolution of the electron population over time for different power levels of the input signal). As a practical example, Fig. 4 shows the electron population over time for the multipactor analysis of the considered WR-90 RW operating at 11 GHz. As can be seen, the number of electrons decays for a power value of 91.9 kW, whereas it grows exponentially for 96.2 kW, thus confirming the threshold value of 94 kW (between the previous two results) automatically detected by SPARK3D. The same procedure must be repeated for any other frequency in the considered range of interest.

For both software tools used in this section (i.e., AIR-RW and SPARK3D), the secondary electron yield (SEY) data used for the aluminum material of the RW under study are collected in Table I. This practical information has been extracted from the corresponding European Cooperation for Standardization (ECSS) document [34].

Fig. 5 shows the multipactor results provided by the two employed software tools for the considered WR-90 RW [see Fig. 1(a)]. As can be seen, small differences (below 0.5 dB) are found between both results in the whole frequency range of interest. However, the very high values obtained (between 60 and 120 kW) are not reasonable in order to perform an experimental validation.

Therefore, in order to reduce the power threshold values to measurable ones, we have considered a second RW where the height dimension of the standard WR-90 is

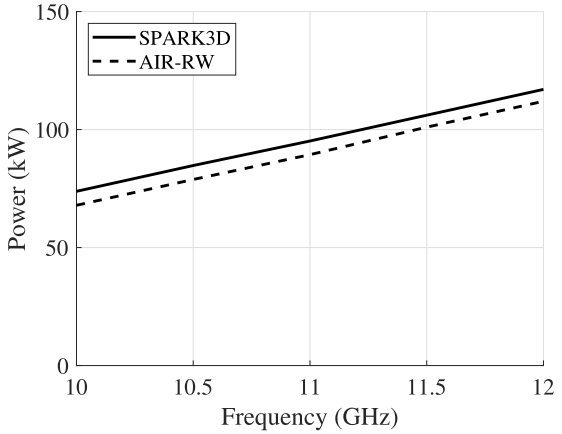

Fig. 5. Multipactor power threshold values (in kW) for the standard WR-90 RW. Results from SPARK3D (with solid line) and obtained with the model in [29] (with dashed line).

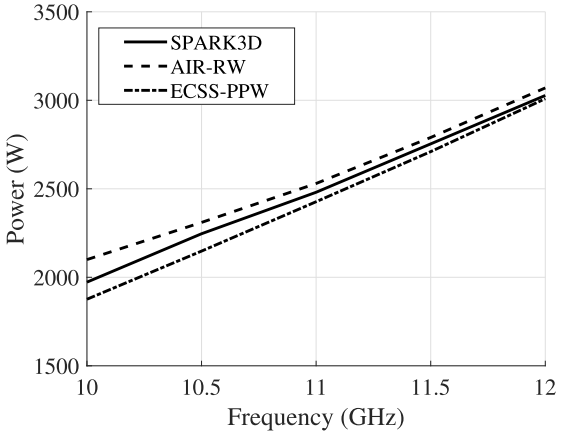

Fig. 6. Multipactor power threshold values (in W) for the WR-90 RW with a reduced waveguide height ($H_G = 0.8$ mm). Results from SPARK3D (with solid line) and results obtained with the model in [29] (dashed line) and with the ECSS model for parallel-plate waveguides (dashed and dotted line).

substantially lowered [i.e., $H_G = 0.8$ mm in Fig. 1(a)]. The new reduced-height waveguide has been analyzed again with the two multipactor analysis tools described before (i.e., SPARK3D and AIR-RW). In addition, the parallel-plate approach model can be also used in this case (since $H_G \ll W_G$), following the procedure detailed in [35]. All these results are successfully compared in Fig. 6, where maximum differences smaller than 225 W can be observed between the three traces. Furthermore, the new power threshold values are now between 2 and 3 kW, which can be measured with the equipment available in the experimental facility.

Thus, in the next section, we will consider a GGW counterpart with a reduced height (see the corresponding geometry in Fig. 7, where $W_G = 22.86$ mm and $H_G = 0.8$ mm).

B. Multipactor Effect in GGW

In this case, due to the more complex geometry of the reduced-height GGW (see Fig. 7), the multipactor analysis will be only performed with the commercial tools SPARK3D and CST Studio Suite, following the same procedure (and software setups) just described before. Again, the material considered is aluminum (whose SEY parameters are given in Table I).

Even though we are considering the zero-gap GGW [30], due to practical manufacturing issues, a very small air gap

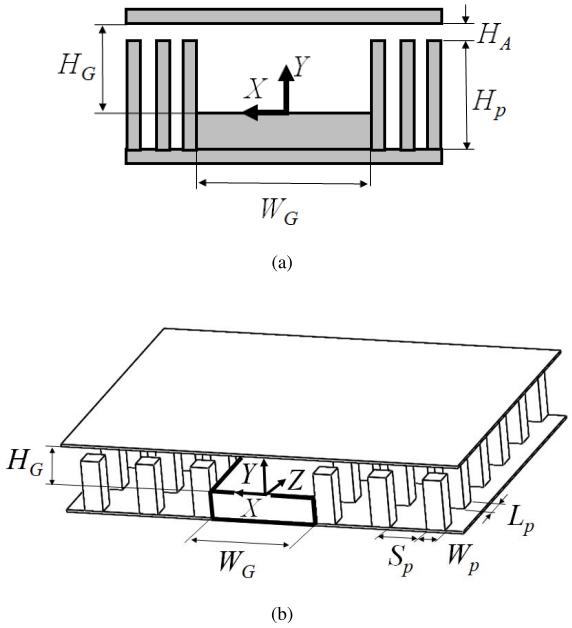

Fig. 7. 2-D and 3-D geometrical representations of the reduced-height GGW in (a) and (b). For the considered case, $W_G = 22.86$ mm, $H_G = 0.8$ mm, $H_p + H_A = 10.16$ mm, $W_P = L_P = 4$ mm, and $S_P = 8$ mm.

(with values of H_A in Fig. 7 of the order of several tens of microns) must be considered. However, these very small gaps are a potential source of additional multipactor discharge, which must be carefully studied and avoided as it has been done next.

For a better understanding of this potential problem, we have first represented the E_Y magnitude of the reduced-height GGW-90 ($W_G = 22.86$ mm and $H_G = 0.8$ mm, considering $H_A = 100$ μm) in Fig. 8. It can be observed that the maximum value in the air gap between the first column of pins and the top metal plate (see the results for line L1). This value is 1.5 times greater than the maximum value of E_Y along the line L2 (located at the center of the reduced-height GGW-90, i.e., at $Y = H_G/2$).

For certain combinations of maximum values of E_Y, RF frequencies, and gap distances (according to the multipactor susceptibility charts for parallel-plate waveguides [4]), the previous EM field distribution (see Fig. 8) can produce low power threshold values (much smaller than the values of Fig. 6 for the RW counterpart). An illustrative example of this undesired phenomenon can be seen in Fig. 9, where the electron cloud is clearly located in the pins area of a reduced-height GGW-90 with an air gap of $H_A = 100$ μm (considering an RF input power level of 730 W).

Therefore, we must perform a parametric study in order to find the optimum value of the air gap (H_A), which ensures that no multipactor discharge will take place between the pins area and the top metal plate in the whole frequency range (from 10 to 12 GHz). Table II shows the results of this multipactor study performed with SPARK3D, where information about the power threshold values (and within parenthesis the multipactor order of the generated discharge) is shown for the reduced-height GGW-90 (considering different values for H_A between 20 and 200 μm).

Based on the susceptibility charts for two parallel plates of aluminum material [5] and considering a gap of 0.8 mm and

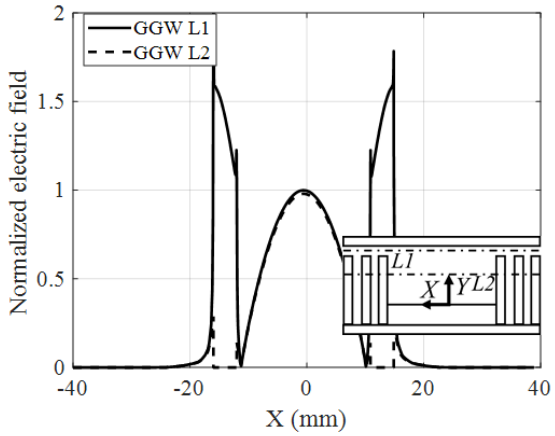

Fig. 8. Comparison of the normalized values of E_Y (computed at 11 GHz) in the reduced-height ($H_G = 0.8$ mm) GGW-90 with a gap $H_A = 100$ μm along the lines L1 (solid line) and L2 (dashed line) located, respectively, at $Y = (H_G - H_A/2)$ and $Y = H_G/2$.

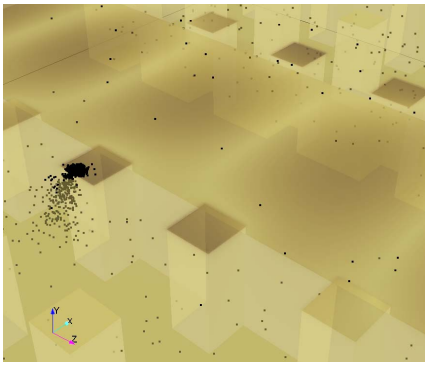

Fig. 9. Electron cloud distribution of a multipactor discharge (RF input power of 730 W at 11 GHz) inside a reduced-height ($H_G = 0.8$ mm) GGW-90 with an air gap of $H_A = 100$ μm.

the frequency range between 10 and 12 GHz (i.e., a set of $f \times d$ values from 8 to 9.6 GHz $\times$ mm), the expected order of the multipactor discharge must always be clearly above 5. Therefore, this condition (a multipactor order larger than 5) is also an indicator that the discharge in a reduced-height GGW is being generated in its central part (with a gap of 0.8 mm) and not in the region of very small gaps.

Observing the results of Table II, we conclude that $H_A = 20$ μm is an optimal choice for the practical implementation of the zero-gap GGW-90 since it is confirmed that, "in such case," the generated discharge is associated with the central gap of the reduced-height ($H_G = 0.8$ mm) GGW. In addition, for $H_A \geq 50$ μm, it can be seen how the power threshold results for each particular frequency are reduced, corresponding to multipactor discharges occurring in very small air gaps.

As an additional confirmation of this optimal choice, i.e., $H_A = 20$ μm, we can see that this value ensures, for frequencies below 12 GHz, that $f \times d \leq 0.24$ GHz $\times$ mm in the very small gaps. Using again the susceptibility charts for aluminum parallel plates in [5], it can be observed that no multipactor discharge (of any order) can ever happen for such low values of the $f \times d$ product. Finally, with further SPARK3D simulations, we have also checked that multipactor results when H_A is below 20 μm keep identical to those for $H_A = 20$ μm in Table II.

From the previous study, it is, therefore, concluded that we will consider a reduced-height GGW-90 with $H_A = 20$ μm.

TABLE II

MULTIPACTOR RESULTS OF THE REDUCED-HEIGHT ($H_G = 0.8$ mm) GGW-90 FOR DIFFERENT FREQUENCIES (IN GHz) AND VALUES OF H_A (IN MICRONS): POWER THRESHOLD VALUES (IN W) AND MULTIPACTOR ORDER (WITHIN PARENTHESIS)

Freq.	**10.0**	**10.5**	**11.0**	**11.5**	**12.0**
$H_A = 20$	2836 (11)	3351 (11)	3914 (13)	4265 (13)	4547 (15)
$H_A = 50$	2601 (11)	2414 (1)	2133 (1)	3445 (1)	3211 (1)
$H_A = 100$	267 (1)	460 (1)	730 (1)	1441 (1)	2039 (1)
$H_A = 200$	592 (3)	1066 (3)	1628 (3)	2414 (13)	3164 (13)

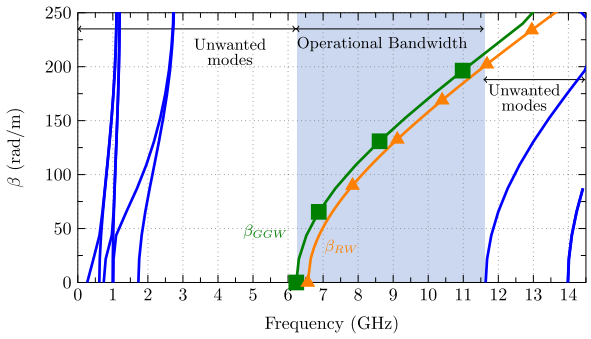

Fig. 10. Dispersion diagram of the reduced-height GGW-90 (unwanted modes with solid lines and fundamental mode with square marks), considering a small air gap of $H_A = 20$ μm in Fig. 7, and the reduced-height WR-90 RW (fundamental mode with triangle marks).

This small value of 20 μm (or even slightly lower) can be guaranteed with accurate manufacturing techniques, as it has been recently achieved in [31]. In addition, through a sensitivity analysis of the reduced-height GGW-90, it has been confirmed that accurate electrical results (with virtually no deviations against design specifications) are obtained for $H_A \leq 20$ μm.

Before proceeding with the multipactor analysis of the reduced-height GGW (see Fig. 7), we have obtained (using again the eigenmode solver of CST Studio Suite) the corresponding dispersion results, considering also a very small air gap ($H_A = 20$ μm). This new dispersion study is shown in Fig. 10, where solid curves correspond to unwanted modes of the considered GGW, and the curves with square and triangle marks are related, respectively, to the fundamental modes of the GGW and RW (with $W_G = 22.86$ mm and $H_G = 0.8$ mm). It can be noticed that some additional unwanted modes appear at very low frequencies since a very small air gap of $H_A = 20$ μm is now considered but without effects on the propagation behavior and operational bandwidth of the fundamental mode. Then, and similar to the zero-gap GGW-90 case (see Fig. 2), it can also be confirmed the equivalence of the reduced-height GGW (with a very small air gap) and the RW counterpart. Thus, we will perform the multipactor analysis of the GGW technology but considering the reduced-height version in order to obtain (as it occurred with the RW counterpart in Section II-A) measurable power threshold values.

Then, the multipactor analysis of the reduced-height ($H_G = 0.8$ mm) GGW-90 (with $H_A = 20$ μm) has been

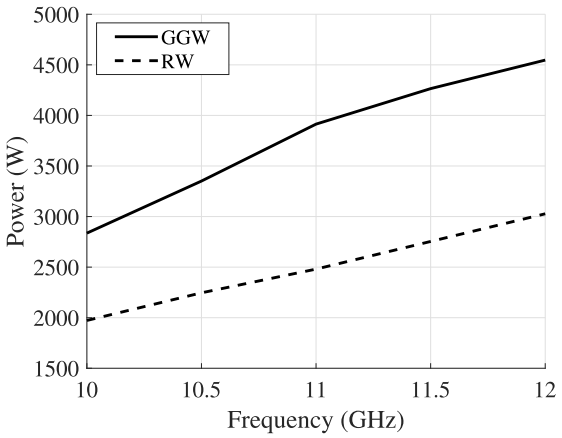

Fig. 11. Multipactor power threshold values (in W) for the GGW-90 with $H_A = 20$ μm (solid line) and for the WR-90 RW (dashed line), both of reduced height ($H_G = 0.8$ mm).

performed from 10 to 12 GHz. As expected, it was confirmed that all observed electron discharges occur in the central part of the waveguide ($X = 0$ mm in Fig. 7), and the multipactor discharges are completely avoided in the critical areas between pins and the top metal plate. The threshold results for the GGW-90 are compared with those for the WR-90 RW case in Fig. 11, where it can be observed that the power threshold values are substantially higher for the GGW (a minimum difference of 860 W with regard to the RW case is observed in all frequencies between 10 and 12 GHz).

III. Design of the E-Plane Transformers With Central Sections in RW and GGW Technologies

Once the reduced-height RW and GGW samples have been designed and analyzed in terms of multipactor effect, rectangular waveguide transformers connecting them to standard WR-90 RW access ports must be added. This is needed in order to perform the experimental validation of the simulated RF discharge results since the output of the corresponding power amplifier available in the testing facility is implemented in the cited standard RW. Both transformers will also enhance the matching conditions between the reduced-height and WR-90 waveguides. For analysis and design purposes, we have employed the software tool CST Studio Suite.

Due to the reduced bandwidth to be covered by the waveguide transformers, i.e., between 10 and 12 GHz, a simple E-plane structure consisting of three RW sections (with a constant width $W_G = 22.86$ mm and different heights) is considered in both cases (see the geometry and main dimensions in Fig. 12). They are based on the classical solution consisting of the cascade connection of quarter-wavelength uniform transmission lines [36], [37]. As can be seen in Fig. 12, the smallest gap (lower height) is always located in the central section of both transformers. Therefore, it can be concluded that multipactor discharges will always take place in the reduced-height RW and GGW under study.

First, we will proceed with the design procedure of the proposed transformer between the reduced-height WR-90 ($b_{\mathrm{RW}} = 0.8$ mm) and the standard WR-90 access port ($b_{\mathrm{WR90}} = 10.16$ mm). The initial values for all design variables (L_{RWi} and b_{RWi}) are obtained as follows: the lengths are equal

TABLE III

Optimized Values (in mm) for the E-Plane Waveguide Transformer Between Reduced-Height ($b_{\mathrm{RW}} = 0.8$ mm) and Standard WR-90 ($b_{\mathrm{WR90}} = 10.16$ mm) RWs

Step	L_{RW}	b_{RW}
1	7.82	7.97
2	7.01	3.53
3	7.78	1.27

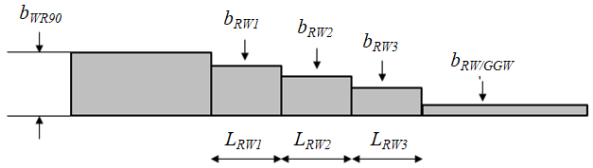

Fig. 12. Geometry and dimensions of the E-plane waveguide transformers (where the variable names are the ones used in Tables III and IV).

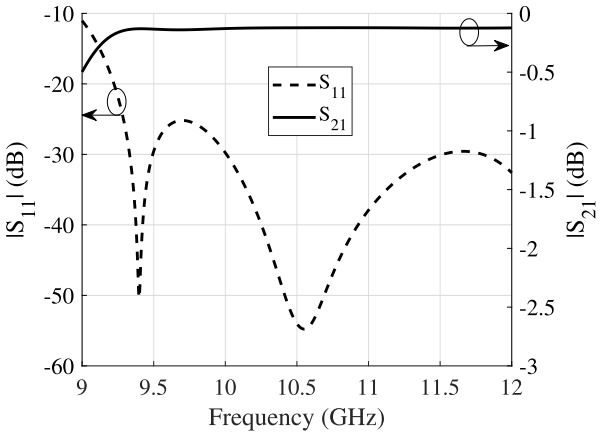

Fig. 13. Simulated response of the designed E-plane transformer between reduced-height and standard WR-90 RWs (in a back-to-back configuration) with a central section of length 70 mm.

to $\lambda_g/4$ at the central frequency of the considered bandwidth (where λ_g is the wavelength in each waveguide section), and the heights (directly related to the modal impedances of each waveguide Section [38]) are chosen to recover the characteristic impedances of the equivalent transformer based on uniform transmission lines [36], [37]. Then, following an optimization process, the final optimum values for all involved design variables are obtained (see Table III). The simulated response of the designed transformer, in a back-to-back configuration with a central section of reduced-height WR-90 RW and length of 70 mm, is shown in Fig. 13. As can be seen, in the frequency range of interest (10–12 GHz), the return losses (RL) are above 30 dB, and the insertion losses (IL) considering aluminum in the simulations are lower than 0.13 dB. In order to validate the good performance of the designed transformer, it has been checked that good matching conditions (i.e., similar results to the ones of Fig. 13) are obtained for a wide set of values for the length of the central waveguide section.

Next, we perform the design of the second transformer between the reduced-height GGW-90 ($b_{\mathrm{GGW}} = 0.8$ mm) and the standard WR-90 access port ($b_{\mathrm{WR90}} = 10.16$ mm). We have chosen again the same topology (and number of sections) of the previous solution (see Fig. 12), considering the same set

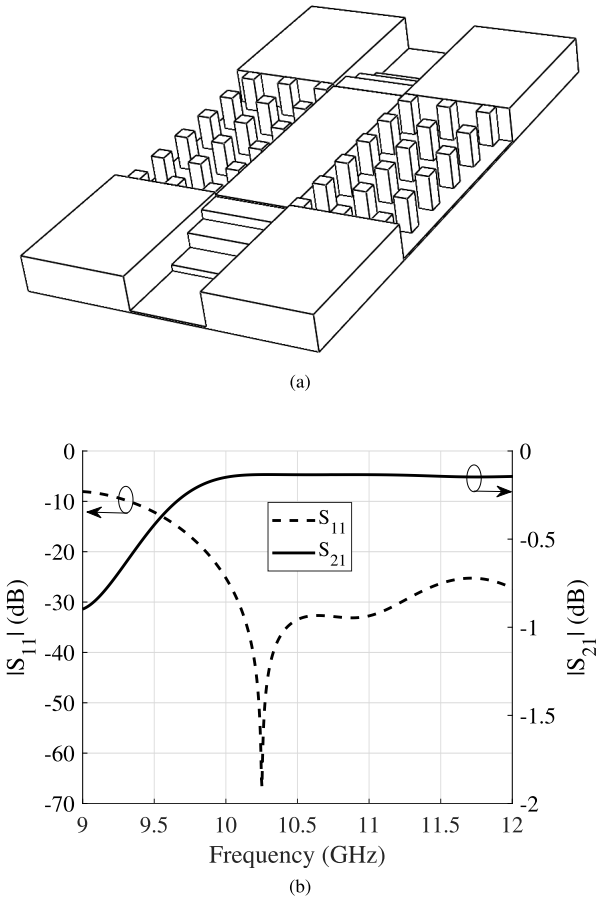

Fig. 14. 3-D internal view of the E-plane waveguide transformer (back-to-back configuration) with a central section of reduced-height GGW-90 (the first and last parts of the GGW are rows of pins) in (a) and its simulated frequency response in (b).

of design variables (the lengths and heights of the three RW sections). The choice of RW technology for implementing the E-plane transformer simplifies the manufacturing process of the complete structure [see Fig. 14(a)].

In this case, as initial values of the design variables of the new transformer (i.e., L_{RWi} and b_{RWi} in Fig. 12), we take the optimal values of the previous solution for the reduced-height WR-90 RW (that can be found in Table III). Even though the GGW has a direct correspondence with its equivalent RW, their propagation characteristics are not exactly identical (very specially in wide frequency ranges) [17]. Therefore, an optimization procedure of all involved design variables of the new transformer must be performed in order to meet all frequency response specifications.

It must be also taken into account that the central section of GGW-90 starts and ends with rows of pins, which are in contact with the metal walls of the adjacent RWs [see Fig. 14(a)]. Proceeding in this way, the discontinuity between the central GGW-90 and the adjacent (front and rear) RWs is minimized, thus helping to reduce the mismatching introduced by the corresponding waveguide steps.

For this second transformer, after the optimization process is concluded, the final set of dimensions can be found in Table IV. The frequency response of the complete structure [back-to-back configuration in Fig. 11(a) with a length of 65 mm for the GGW] is displayed in Fig. 14(b). In the bandwidth of interest (10–12 GHz), the RL and IL values are above 25 dB and below 0.16 dB, respectively. We have also confirmed that good matching conditions are preserved for different length values of the GGW-90 central section.

TABLE IV

OPTIMIZED VALUES (IN mm) FOR THE E-PLANE WAVEGUIDE TRANSFORMER BETWEEN GGW SECTION WITH REDUCED-HEIGHT ($b_{\mathrm{GGW}} = 0.8$ mm) AND STANDARD WR-90 ($b_{\mathrm{WR90}} = 10.16$ mm) RW

Step	L_{RW}	b_{RW}
1	9.06	8.36
2	7.53	4.03
3	7.18	1.27

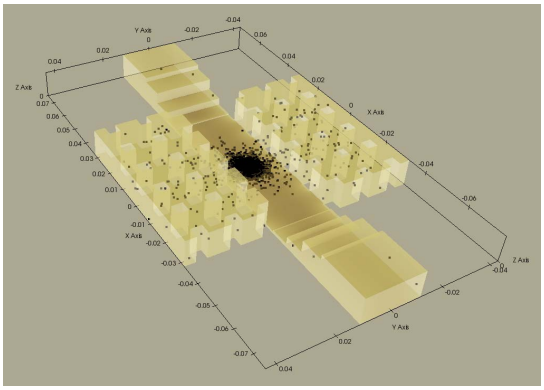

Fig. 15. Electron cloud distribution of a multipactor discharge (RF input power of 3.9 kW at 11 GHz) inside the transformer with a reduced-height ($H_G = 0.8$ mm) GGW-90 (air gap of $H_A = 20$ μm) central sections.

TABLE V

MULTIPACTOR THRESHOLD VOLTAGES (IN V) FOR THE REDUCED HEIGHT WR-90 RW AND GGW-90

Frequency (GHz)	**10.0**	**10.5**	**11.0**	**11.5**	**12.0**
TRF-GGW-TRF	444	461	488	506	522
TRF-RW-TRF	375	394	414	426	436

Data extracted from the susceptibility charts of Fig.16(b)

IV. MULTIPACTOR ANALYSIS IN THE E-PLANE TRANSFORMERS WITH CENTRAL SECTIONS IN RW AND GGW TECHNOLOGIES

Once the two E-plane transformers (TRFs) are completely designed, we can perform the comparative multipactor study of the two reduced-height waveguide samples considered in Section II, i.e., the WR-90 RW and GGW-90 (both with $H_G = 0.8$ mm). For the GGW-case, as it was detailed in Section II-B, an air gap of $H_A = 20$ μm was chosen, which is small enough to avoid the multipactor effect in the pins area of the zero-gap GGW.

In this study, we have used the software tools SPARK3D and CST Studio Suite to perform the multipactor analysis of both RW transformers (i.e., the ones with RW and GGW central sections). For both cases, all the high-power simulations performed have shown that the discharge electron clouds are always located in the corresponding reduced-height waveguide samples. This can be clearly seen in Fig. 15, where the multipactor effect is taking place around the central area of the GGW-90 section.

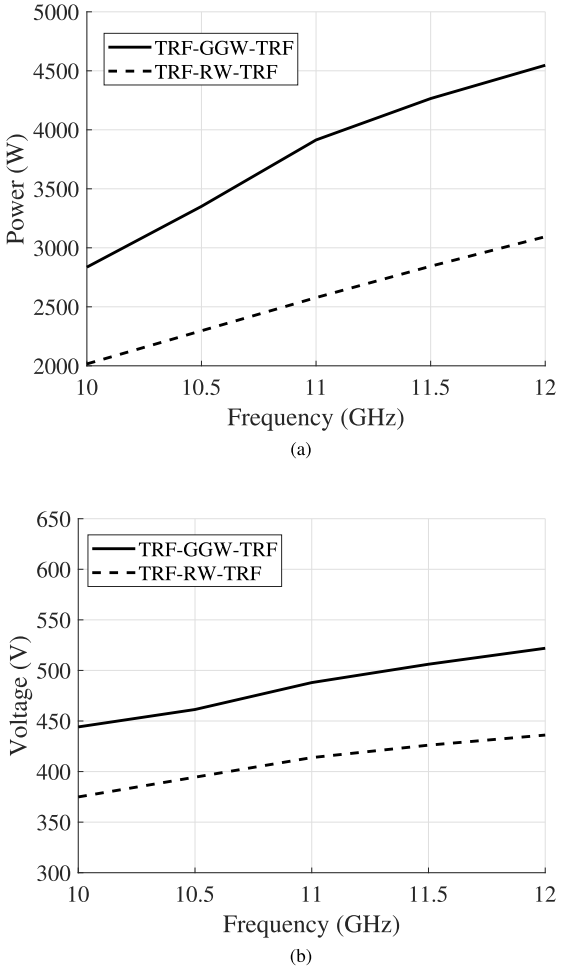

Fig. 16. Multipactor threshold values (in W) for the reduced-height ($H_G = 0.8$ mm) GGW-90 with $H_A = 20$ μm (solid lines) and the WR-90 RW (dashed lines) including transformers (back-to-back configuration) in (a) and susceptibility charts of both waveguides in (b).

The power threshold results for the two E-plane transformers (in a back-to-back configuration), with the reduced-height WR-90 and GGW-90 central sections, are compared in Fig. 16(a). As expected, both results are very similar to the ones of Fig. 11 (waveguide samples without transformers), which confirms the good performance of both designed RW transformers. Likewise, we can observe in Fig. 16(a) that the threshold values are considerably higher for the GGW in all considered frequencies between 10 and 12 GHz (with a minimum difference of 820 W at 10 GHz).

Next, we have obtained the multipactor susceptibility charts of both considered waveguides (reduced-height WR-90 RW and GGW-90), which are included in Fig. 16(b). The multipactor breakdown voltages have been computed, as detailed in [33], within the central sections of the two E-plane transformers in a back-to-back configuration. The specific values for certain frequencies of the considered bandwidth (10–12 GHz) are collected in Table V. All these results confirm, again, the better performance of the GGW over RW in terms of the RF multipactor breakdown effect.

V. Experimental Results

The two E-plane transformers, whose central sections include the designed RW and GGW samples, have been

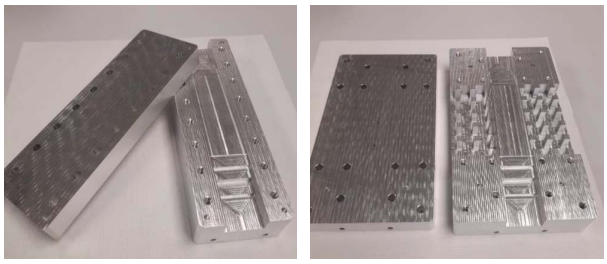

Fig. 17. View of the two manufactured transformers (top and body in each case) with a central section in RW (left) and GGW (right) technologies.

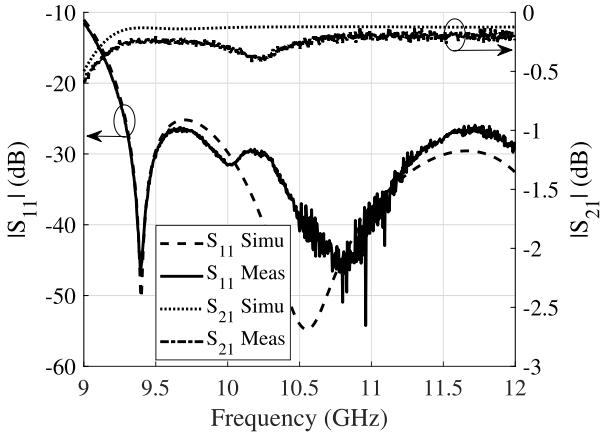

Fig. 18. Measured and simulated responses of the transformer (in back-to-back configuration) with central section in RW technology.

manufactured in aluminum employing a milling technique (as can be seen, with a back-to-back configuration, in Fig. 17). Both simulated and measured frequency responses are shown in Fig. 18 (for the RW central section) and Fig. 19 (for the GGW case). In general, a good agreement between simulated and measured data is observed. Some few discrepancies (in particular, a frequency shift of the S11 parameter for the GGW case) are attributed to small manufacturing tolerances. It can also be observed a slight difference (around 0.25 dB at frequencies above 10.5 GHz) between the measured IL values for the two transformers (with GGW and RW central samples). For the GGW case, additional ohmic losses can be present due to the surface currents induced in the metal pins by residual EM fields located in the very small air gap regions. However, taking into account that the experimental multipactor study is performed in the frequency range of 10.5–12 GHz, it can be concluded that both transformer responses are compliant with the requirements needed (in terms of both IL and RL levels) for performing the high-power tests.

As indicated before, the multipactor experimental campaign has been performed at the High Power RF Space Laboratory of ESA and VSC, where all necessary equipment (in particular, power amplifiers for the selected Ku-band frequency range) is available. A standard experimental setup (according to [35]) was assembled for performing the multipactor measurements of both manufactured prototypes. For detection of the potential RF discharges, the global detection methods used were the phase nulling and the third harmonic systems since they are very effective with single carrier continuous wave signals. In addition, a local detection method (based on electrometers detecting the electron population growth in the vicinity of critical areas of the samples) was also employed. Two different

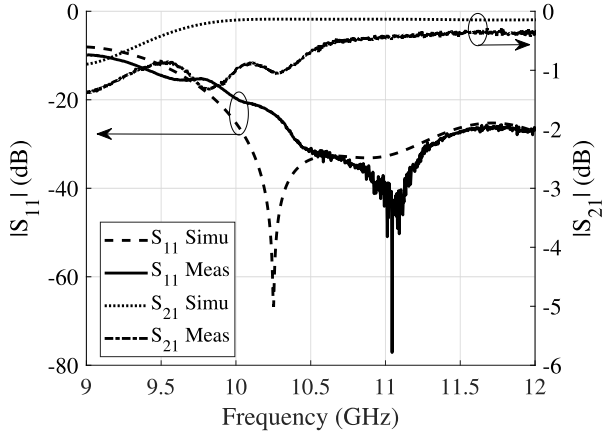

Fig. 19. Measured and simulated responses of the transformer (in back-to-back configuration) with central section in GGW technology.

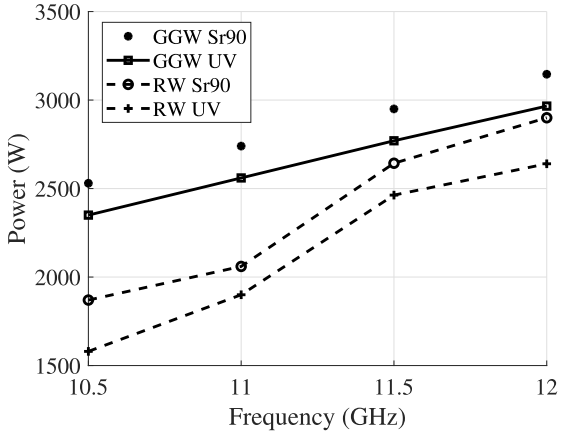

Fig. 20. Multipactor power threshold values (in W) for the transformers with RW and GGW central sections using electron sources of Sr90 and UV light.

TABLE VI

EXPERIMENTAL AND SIMULATED RESULTS FOR MULTIPACTOR POWER THRESHOLD (IN W) FOR THE TRANSFORMERS WITH RW AND GGW CENTRAL SECTIONS

Frequency (GHz)	**10.5**	**11.0**	**11.5**	**12.0**
RW Sr90	1870	2060	2643	2900
RW UV	1580	1900	2463	2640
RW SPARK3D	2246	2480	2754	3027
GGW Sr90	2530	2740[a]	2950[b]	3146[c]
GGW UV	2350	2560	2770	2966
GGW SPARK3D	3351	3914	4265	4547

[a,b,c] Values obtained by linear extrapolation

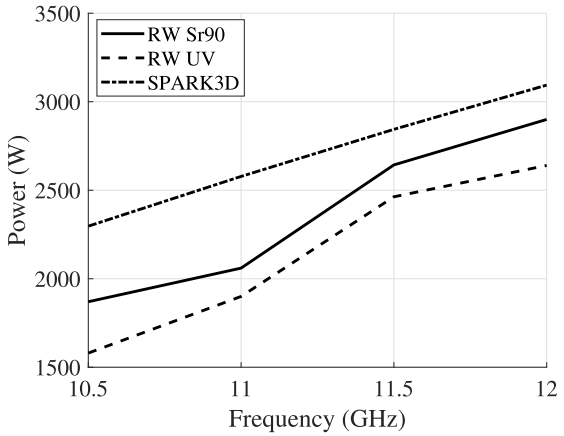

Fig. 21. Comparison of simulated (SPARK3D) and measured results, using Sr90 (RW Sr90) and UV light (RW UV) electron sources, of the transformer with an RW central section.

electron sources have been used for performing the experimental measurements of the multipactor effect. The first one employs a radioactive isotope of Strontium (Sr90). The second source is based on the injection of ultraviolet (UV) light within the sample under test, thus illuminating the critical area where the RF multipactor discharge is expected to occur.

Table VI includes the experimental results for multipactor power threshold values (in W) of both transformers (with RW and GGW samples) obtained with the two-electron sources outlined before (i.e., Sr90 and UV light). The same results are graphically compared in Fig. 20. As can be seen from the results of the RW sample, both sets of measured data (RW Sr90 and RW UV) follow a similar trend, but the values obtained with the Sr90 source are higher. This small difference may be attributed to the fact that electrons radiated by the Sr90 source must penetrate the aluminum walls of the manufactured prototype. Even though the thickness of such metal walls is low (typically less than 1 mm), the number of available primary electrons will be reduced somehow, which is not the case with the UV light source (located inside the waveguide device under test).

In the case of the GGW sample, measurements have been performed for all considered frequency points (10.5, 11, 11.5, and 12 GHz) using the UV source, whereas experimental data with Sr90 source have been obtained at 10.5 GHz (due to the large set of measured data already available). Observing a similar difference between the measured data (GGW Sr90 and GGW UV) at 10.5 GHz as the one in the RW case, the rest of the values have been adjusted following a linear trend (the same one observed for the GGW results with UV light source). This has also been indicated in the footnote of Table VI.

Comparing now the experimental results for the RW and GGW samples, using for each comparison the same type of electron source (i.e., UV light and Sr90, respectively), we can confirm that GGW outperforms RW in terms of RF multipactor breakdown in the whole frequency range. For instance, using the UV light source, the positive differences between threshold power levels of GGW and RW samples are of 770 (at 10.5 GHz) and 326 W (at 12 GHz). This fully validates the same conclusion reached with the simulated results of Sections II and III, which was also advanced with the observation of the different values and distributions of the electric fields in both technologies (remember Fig. 3).

Figs. 21 and 22 compare the breakdown power levels of simulated results (obtained with SPARK3D) and experimental data (using Sr90 and UV light electron sources) for the two transformers with RW (see Fig. 21) and GGW (see Fig. 22) central sections. In both cases, the simulated results are above the two sets of measured data, which can be attributed to the real SEY values of the aluminum material employed in the fabrication of the two prototypes. Nevertheless, the experimental results for both transformers (with RW and GGW central elements) can be directly compared since both come

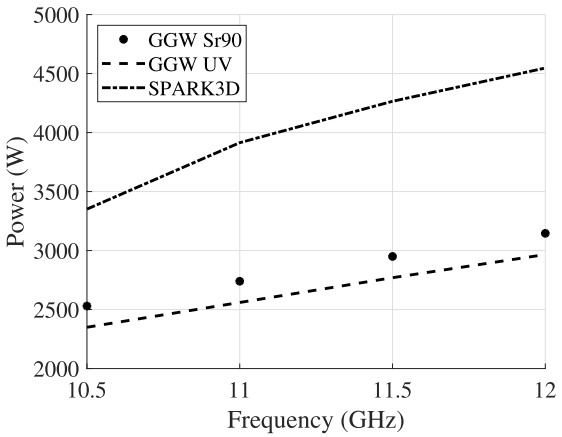

Fig. 22. Comparison of simulated (SPARK3D) and measured results, using Sr90 (GGW Sr90) and UV light (GGW UV) electron sources, of the transformer with a GGW central section.

from the same batch (they were built using the same material, manufacturing process, and machinery).

VI. Practical Considerations

In this section, and after completing a detailed study on the multipactor effect in the GGW technology, including both theoretical results (obtained with available commercial software tools) and experimental validation data, several conclusions and related practical aspects are outlined. We will discuss the most relevant parameters affecting the multipactor discharge in this technology, making special emphasis on the practical considerations for designing future components in GGW technology with a good response in terms of RF discharge effects. Prospects for the potential use of this technology in the millimeter-wave frequency range, and particularly for high-power applications, are discussed next.

In recent years, several wireless applications in the millimeter-wave frequency range (with operational frequencies above 30 GHz) are emerging, where high data rate communication services can be provided due to the available bandwidth [39]. Among them, we can mention the next 5G wireless communication systems using the Ka-band, as well as scanning applications and future indoor wireless systems implemented at 60 GHz (Q- and V-bands) and even in the E-band (60–90 GHz). Due to the high attenuation of the radio signals in these frequency spectrum bands, low insertion loss components and their integration in single physical platforms (avoiding packaging and leakage issues) are demanded. In this context, the GGW technology has been recently employed for implementing integrated millimeter-wave transceivers [40], including radiator elements, feeding networks, active circuits, filters, diplexers, and orthomode transducers [41]–[43]. The practical use of this technology has also been demonstrated with the design and realization of a complete E-band radio front end [44], where a system packaging solution integrating passive and active circuits is addressed [45]. In the previous applications, and particularly in other potential areas of use of the GGW technology, for instance, with radar (both aerial and terrestrial) systems and satellite communication links, the transmission of high-power signals will be needed. Thus, the performance of this technology in terms of RF discharge effects (such as multipactor and corona) must be researched and duly considered.

Based on the theoretical and experimental results included in this work, it can be confirmed that GGW technology behaves, in terms of multipactor effect, very similarly (or slightly better) than the well-known standard RW counterpart. Nevertheless, it must be pointed out that the results of this work correspond to simple sections of empty waveguides in both technologies. In order to perform a more complete comparative study, further research work should be performed in this area of multipactor, for instance, considering the behavior of more complex passive components (such as low-pass and bandpass filters, widely used in the output stage of satellite communication payloads). The good results obtained in this work (of practical interest, due to the considered frequency range, for satellite down-link channels operating in the Ku-band) should also be confirmed at higher frequency bands (such as the Ka-, Q-, and V-bands of great interest in present and future satellite communication systems). At these higher frequencies, GGW can be a competitive technological solution, having already shown very promising results in terms of electrical response and mechanical robustness at the V-band [21].

In general, RF multipactor discharges are strongly dependent on the magnitude of the EM fields between two parallel metal surfaces, and the gap distance between them and the frequency value of the RF continuous-wave excitation signal (the so-called $f \times d$ product), as well as on the SEY properties of the involved materials [1]. Multipactor susceptibility charts (giving threshold values in terms of $f \times d$) have been provided based on theoretical models and empirical data (as shown in [2] and [4]) for the parallel-plate case. More recently, and making use of available commercial tools for computing the EM fields and tracking the resulting electron motion, more accurate results for estimating the power threshold values have been obtained for RW structures [7]. Based on this more accurate approach, we have performed a detailed multipactor study of the GGW technology, having identified relevant practical aspects to be discussed next.

First, and taking into account that the GGW technology behaves like an equivalent RW counterpart, we have computed the electric fields in these two waveguides (see Fig. 3) to confirm the location of the most critical region for the multipactor discharge (where the electric field is higher). From this comparative study, we have already concluded that the electric field distribution and the maximum value are more convenient for obtaining higher multipactor threshold values in the GGW technology. However, and as it happened with the multipactor study in RW technology [7], we must also consider a reduced-height GGW in order to obtain measurable power threshold results. For this purpose, we have proposed the reduced-height GGW, having proved it is equivalent to an RW counterpart with the same dimensions. Then, the multipactor study has been focused on these reduced-height waveguides with the aim of completing the theoretical results with experimental data to be measured using available high-power equipment.

Next, a very relevant aspect affecting the multipactor results for the considered GGW has been identified and studied in

detail. The classical implementation of the GGW technology is realized allowing a certain gap (with values of several tenths, or even units, of millimeters) between the top metal plate and the one including the bed of periodic pins [20], where maximum values of the electric field can be present (as shown in Fig. 8 of this work). In such a case, the authors have checked that the power threshold values for the GGW are strongly reduced due to the emergence of the multipactor effect in the identified small gap critical regions. For avoiding this potential limitation, authors have proposed to use the zero-gap implementation of the GGW technology [30], where air gaps of 20 microns (or less) can be practically guaranteed [31]. A parametric study of the multipactor effect (described in Section II-B) has confirmed that, for small air gaps (of 20 microns or less), the RF discharge will not appear in these problematic areas, thus recovering power threshold values for the GGW even higher than for the standard RW counterpart.

The previous conclusion is extremely relevant from a practical point of view since it has raised a critical parameter for the design of future components based on the GGW technology in order to avoid a drastic reduction of the power threshold values for the multipactor effect. The proposed solution, i.e., the zero-gap GGW considering also small air gaps due to practical manufacturing issues, has been confirmed (both theoretically and also with the experimental results in Section V) to behave as well as the classical RW counterpart.

Finally, it must be remarked that no other previous studies about multipactor effect in the GGW technology are found in the technical literature. However, and as it was indicated in the Introduction, simulated results for another RF discharge effect (called corona or gas breakdown which, contrarily to multipactor, requires some pressure inside the component) can be found in [28]. In this complementary work, and in order to avoid the previously cited problem of higher electric fields in small gap regions (of several tenths of millimeters) around the pins (thus also limiting the corona breakdown power level), an optimization of the dimensions of the bed of periodic pins is successfully proposed. Such an interesting solution, which may also involve a reduction of the operational bandwidth of the GGW, will not be useful in our case since the residual electric fields in the cited small air gaps can still generate multipactor with a reduced power threshold value.

From previous paragraphs, all relevant parameters affecting the power threshold values of multipactor effect in the promising GGW technology have been identified and thoroughly studied. Besides, practical considerations to be followed with the implementation of this technology, with the aim of providing a satisfactory response in terms of multipactor effect, have also been discussed.

VII. Conclusion

In this work, a theoretical and experimental comparative study of the multipactor effect in RW and GGW technologies has been performed. For these purposes, simulated results (using different models and commercial software tools) are shown for standard and reduced-height RW and GGW samples. The zero-gap GGW implementation (considering that a very small air gap will be always present) has been chosen, thus avoiding the potential risk of suffering multipactor (with low threshold values) in the pins area of the periodic hosting structure. For validation purposes, two RW transformers with reduced-height central sections (implemented in RW and GGW technologies) have been successfully designed and manufactured. In both cases, it has been confirmed that potential RF discharges can only occur in the central sections hosting the RW and GGW samples under study. Experimental results (of both electrical responses and high vacuum RF discharges) fully confirm all previously simulated results, as well as the outperformance of the GGW technology in terms of the multipactor effect.

Acknowledgment

The authors would like to thank the European High Power RF Space Laboratory of the European Space Agency and the Val Space Consortium for contributing with its installations—Laboratory cofunded by the European Regional Development Fund—a way of making Europe.

References

[1] J. R. M. Vaughan, "Multipactor," *IEEE Trans. Electron Devices*, vol. ED-35, no. 7, pp. 1172–1180, Jul. 1988.

[2] A. J. Hatch and H. B. Williams, "Multipacting modes of high-frequency gaseous breakdown," *Phys. Rev.*, vol. 112, pp. 681–685, Nov. 1958.

[3] M. Jiménez *et al.*, "Analysis of the electromagnetic radiation generated by a multipactor discharge occurring within a microwave passive component," *J. Phys. D, Appl. Phys.*, vol. 43, no. 39, Oct. 2010, Art. no. 395501.

[4] A. J. Hatch and H. B. Williams, "The secondary electron resonance mechanism of low-pressure high-frequency gas breakdown," *J. Appl. Phys.*, vol. 25, no. 4, pp. 417–423, Apr. 1954.

[5] A. Wood and J. Petit, "Diagnostic investigations into the multipactor effect, susceptibility zone measurements and parameters affecting a discharge," ESA/ESTEC, Noordwijk, The Netherlands, Work. Paper 1556, Nov. 1989.

[6] V. E. Semenov, E. I. Rakova, D. Anderson, M. Lisak, and J. Puech, "Multipactor in rectangular waveguides," *Phys. Plasmas*, vol. 14, no. 3, Mar. 2007, Art. no. 033501.

[7] C. Vicente *et al.*, "Multipactor breakdown prediction in rectangular waveguide based components," in *IEEE MTT-S Int. Microw. Symp. Dig.*, Jun. 2005, pp. 1055–1058.

[8] E. Chojnacki, "Simulations of a multipactor-inhibited waveguide geometry," *Phys. Rev. Special Topics Accel. Beams*, vol. 3, no. 3, Mar. 2000, Art. no. 032001.

[9] A. M. Pérez, V. E. Boria, B. Gimeno, S. Anza, C. Vicente, and J. Gil, "Multipactor analysis in circular waveguides," *J. Electromagn. Waves Appl.*, vol. 23, nos. 11–12, pp. 1575–1583, 2009.

[10] A. Frotanpour, B. Gimeno, and S. Esfandiarpour, "Multipactor in dualmode elliptical waveguide," in *Proc. 31st Int. Rev. Prog. Appl. Comput. Electromagn. (ACES)*, Williamsburg, VA, USA, May 2015, pp. 1–2.

[11] D. Gonzalez-Iglesias *et al.*, "Multipactor susceptibility charts for ridge and multiridge waveguides," *IEEE Trans. Electron Devices*, vol. 59, no. 12, pp. 3601–3607, Dec. 2012.

[12] A. M. Pérez *et al.*, "Prediction of multipactor breakdown thresholds in coaxial transmission lines for traveling, standing, and mixed waves," *IEEE Trans. Plasma Sci.*, vol. 37, no. 10, pp. 2031–2040, Oct. 2009.

[13] D. González-Iglesias, O. Monerris, B. G. Martínez, M. E. Díaz, V. E. Boria, and P. Martín-Iglesias, "Multipactor RF breakdown in coaxial transmission lines with digitally modulated signals," *IEEE Trans. Electron Devices*, vol. 63, no. 10, pp. 4096–4103, Oct. 2016.

[14] V. E. Semenov *et al.*, "Simulations of multipactor thresholds in shielded microstrip lines," *J. Phys. D, Appl. Phys.*, vol. 42, no. 20, Sep. 2009, Art. no. 205204.

[15] P.-S. Kildal, E. Alfonso, A. Valero-Nogueira, and E. Rajo-Iglesias, "Local metamaterial-based waveguides in gaps between parallel metal plates," *IEEE Antennas Wireless Propag. Lett.*, vol. 8, pp. 84–87, 2009.

[16] A. Valero-Nogueira, M. Baquero, J. I. Herranz, J. Domenech, E. Alfonso, and A. Vila, "Gap waveguides using a suspended strip on a bed of nails," *IEEE Antennas Wireless Propag. Lett.*, vol. 10, pp. 1006–1009, 2011.
[17] A. Berenguer, V. Fusco, D. E. Zelenchuk, D. Sánchez-Escuderos, M. Baquero-Escudero, and V. E. Boria-Esbert, "Propagation characteristics of groove gap waveguide below and above cutoff," *IEEE Trans. Microw. Theory Techn.*, vol. 64, no. 1, pp. 27–36, Jan. 2016.
[18] M. G. Silveirinha, C. A. Fernandes, and J. R. Costa, "Electromagnetic characterization of textured surfaces formed by metallic pins," *IEEE Trans. Antennas Propag.*, vol. 56, no. 2, pp. 405–415, Feb. 2008.
[19] A. Valero, E. Alfonso, J. I. Herranz, and P. Simon, "Experimental demonstration of local quasi-TEM gap modes in single-hard-wall waveguides," *IEEE Microw. Wireless Compon. Lett.*, vol. 19, no. 9, p. 536—538, Sep. 2009.
[20] E. Rajo-Iglesias and P. S. Kildal, "Numerical studies of bandwidth of parallel-plate cut-off realised by a bed of nails, corrugations and mushroom-type electromagnetic bandgap for use in gap waveguides," *IET Microw., Antennas Propag.*, vol. 5, no. 3, p. 282—289, Feb. 2011.
[21] A. Berenguer, D. Sánchez-Escuderos, B. Bernardo-Clemente, M. Baquero-Escudero, and V. E. Boria, "Groove gap waveguide as an alternative to rectangular waveguide for H-plane components," *Electron. Lett.*, vol. 52, no. 11, pp. 939–941, May 2016.
[22] M. Rezaee, A. U. Zaman, and P.-S. Kildal, "V-band groove gap waveguide diplexer," in *Proc. 9th Eur. Conf. Antennas Propag. (EuCAP)*, Apr. 2015, pp. 1–4.
[23] Y. Quan, J. Yang, H. Wang, and A. U. Zaman, "A simple asymmetric orthomode transducer based on groove gap waveguide," *IEEE Microw. Wireless Compon. Lett.*, vol. 30, no. 10, pp. 953–956, Oct. 2020.
[24] A. Farahbakhsh, "Ka-band coplanar Magic-T based on gap waveguide technology," *IEEE Microw. Wireless Compon. Lett.*, vol. 30, no. 9, pp. 853–856, Sep. 2020.
[25] Y. Shi, W. Feng, X. Jiang, Q. Xue, and W. Che, "Half-air-filled ball-grid-array-based substrate-integrated groove-gap waveguide and its transition to microstrip at W-Band," *IEEE Trans. Microw. Theory Techn.*, vol. 68, no. 12, pp. 5145–5153, Dec. 2020.
[26] R. F. J. Broas, D. F. Sievenpiper, and E. Yablonovitch, "A high-impedance ground plane applied to a cellphone handset geometry," *IEEE Trans. Microw. Theory Tech.*, vol. 49, no. 7, pp. 1262–1265, Jul. 2001.
[27] A. P. Feresidis, G. Goussetis, S. Wang, and J. C. Vardaxoglou, "Artificial magnetic conductor surfaces and their application to low-profile high-gain planar antennas," *IEEE Trans. Antennas Propag.*, vol. 53, no. 1, pp. 209–215, Jan. 2005.
[28] A. Morales-Hernandez, M. Ferrando-Rocher, M. A. Sanchez-Soriano, S. Marini, and V. E. Boria, "Design strategy and considerations to improve corona discharge breakdown in groove gap waveguides," in *Proc. 15th Eur. Conf. Antennas Propag. (EuCAP)*, Mar. 2021, pp. 1–5.
[29] A. Berenguer, A. Coves, F. Mesa, E. Bronchalo, and B. Gimeno, "Analysis of multipactor effect in a partially dielectric-loaded rectangular waveguide," *IEEE Trans. Plasma Sci.*, vol. 47, no. 1, pp. 259–265, Jan. 2019.
[30] S. I. Shamseldin, "Analysis and design of microwave devices based on ridge gap waveguide technology," Ph.D. dissertation, Dept. Elect. Comput. Eng., Concordia Univ. Montréal, Montréal, QC, Canada, Aug. 2016.
[31] M. Baquero-Escudero, A. Valero-Nogueira, M. Ferrando-Rocher, B. Bernardo-Clemente, and V. E. Boria-Esbert, "Compact combline filter embedded in a bed of nails," *IEEE Trans. Microw. Theory Techn.*, vol. 67, no. 4, pp. 1461–1471, Apr. 2019.
[32] E. Rajo-Iglesias and P.-S. Kildal, "Groove gap waveguide: A rectangular waveguide between contactless metal plates enabled by parallel-plate cut-off," in *Proc. 4th Eur. Conf. Antennas Propag.*, Barcelona, Spain, Apr. 2010, pp. 1–4.
[33] J. Vague *et al.*, "Multipactor effect characterization of dielectric materials for space applications," *IEEE Trans. Microw. Theory Techn.*, vol. 66, no. 8, pp. 3644–3655, Aug. 2018.
[34] *Multipacting Design Test*, document ECSS-E-ST-20-01C, European Cooperation for Space Standarization (ECSS), ESA-ESTEC, ESA Publication Division, Amsterdam, The Netherlands, Jun. 2020.
[35] *Multipacting Handbook*, document ECSS-E-HB-20-01A, European Cooperation for Space Standarization (ECSS), ESA-ESTEC, ESA Publication Division, Amsterdam, The Netherlands, Jun. 2020.
[36] R. E. Collin, "Theory and design of wide-band multisection quarter-wave transformers," *Proc. IRE*, vol. 43, no. 2, pp. 179–185, Feb. 1955.
[37] G. Matthaei, L. Young, and E. M. T. Jones, *Microwave Filters Impedance Matching Networks and Coupling Structures*. Norwood, MA. USA: Artech House, 1980.
[38] N. Marcuvitz, *Waveguide Handbook*. New York, NY, USA: McGraw-Hill, 1955.
[39] T. S. Rappaport, Y. Xing, G. R. MacCartney, A. F. Molisch, E. Mellios, and J. Zhang, "Overview of millimeter wave communications for fifth-generation (5G) wireless networks—With a focus on propagation models," *IEEE Trans. Antennas Propag.*, vol. 65, no. 12, pp. 6213–6230, Dec. 2017.
[40] A. Vosoogh, M. S. Sorkherizi, A. U. Zaman, J. Yang, and A. A. Kishk, "An integrated Ka-band diplexer-antenna array module based on gap waveguide technology with simple mechanical assembly and no electrical contact requirements," *IEEE Trans. Microw. Theory Techn.*, vol. 66, no. 2, pp. 962–972, Feb. 2018.
[41] A. Farahbakhsh, D. Zarifi, and A. U. Zaman, "60-GHz groove gap waveguide based wideband H-plane power dividers and transitions: For use in high-gain slot array antenna," *IEEE Trans. Microw. Theory Techn.*, vol. 65, no. 11, pp. 4111–4121, Nov. 2017.
[42] M. Rezaee and A. U. Zaman, "Groove gap waveguide filter based on horizontally polarized resonators for V-Band applications," *IEEE Trans. Microw. Theory Techn.*, vol. 68, no. 7, pp. 2601–2609, Jul. 2020.
[43] M. A. Abdelaal and A. A. Kishk, "Ka-band 3-D-printed wideband groove gap waveguide orthomode transducer," *IEEE Trans. Microw. Theory Techn.*, vol. 67, no. 8, pp. 3361–3369, Aug. 2019.
[44] A. Vosoogh *et al.*, "Compact integrated full-duplex gap waveguide-based radio front end for multi-Gbit/s point-to-point backhaul links at E-band," *IEEE Trans. Microw. Theory Techn.*, vol. 67, no. 9, pp. 3783–3797, Sep. 2019.
[45] U. Nandi, A. U. Zaman, A. Vosoogh, and J. Yang, "Novel millimeter wave transition from microstrip line to groove gap waveguide for MMIC packaging and antenna integration," *IEEE Microw. Wireless Compon. Lett.*, vol. 27, no. 8, pp. 691–693, Aug. 2017.

José Joaquín Vague was born in Valencia, Spain, in 1970. He received the Ingeniería Electrónica degree from the Universitat de València, Valencia, in 2003, where he is currently pursuing the Ph.D. degree in electronic engineering.

He is currently a Technical Researcher in charge of several laboratories with the Departamento de Comunicaciones, Universitat Politècnica de València (UPV), Valencia. His current research interest includes the design of microwave passive devices, especially in filters and nonreciprocal devices, and the improvement in manufacturing processes in the RF and microwave range.

Irene Asensio was born in Segorbe (Castellón), Spain, in 1999. She received the Ingeniería de Telecomunicaciones degree from the Universitat Politècnica de València, Valencia, Spain, in 2021.

Her current research interest includes the design of microwave passive devices, especially in filters and nonreciprocal devices, and the improvement in manufacturing processes in the RF and microwave range.

Ángela Coves (Senior Member, IEEE) received the Licenciado and Ph.D. degrees in physics from the Universitat de València, Valencia, Spain, in 1999 and 2004, respectively.

In 2001, she joined the Departamento de Ingeniería de Comunicaciones, Universidad Miguel Hernández de Elche, Elche, Spain, where she became a Full Professor in 2021. Her current research interests include the analysis and design of microwave passive components, periodic structures, and RF breakdown high-power effects.

Ángel A. San Blas was born in Fortaleny, Valencia, Spain, in 1976. He received the Ingeniero de Telecomunicación and the Doctor Ingeniero de Telecomunicación degrees from the Universitat Politècnica de València, Valencia, Spain, in 2000 and 2008, respectively.

From 2001 to 2002, he was a Researcher Assistant with the Departamento de Comunicaciones, Universitat Politècnica de València, where he was involved in the development of simulation tools for the analysis and design of waveguide devices. From November 2001 to March 2002, he was a Researcher with the Department of Electronics, Università degli Studi di Pavia, Pavia, Italy, where he was involved in the research project Millimeter-Wave and Microwave Components Design Framework for Ground and Space Multimedia Network (V European Framework Project). Since 2003, he has been an Associate Professor with the Departamento de Ingeniería de Comunicaciones, Universidad Miguel Hernández de Elche, Elche, Spain. His current research interests include the analysis and design of passive waveguide components for satellite communication systems.

Dr. San-Blas also serves as an Editorial Board Member (Area Editor) for the *International Journal of Electronics and Communications* (Elsevier).

Marta Reglero was born in Alicante, Spain, in 1982. She received the Ingeniería de Telecomunicaciones degree from the Universitat Politècnica de València (UPV), Valencia, Spain, in 2008.

From 2006 to 2008, she was a Fellow Researcher with the Institute of Telecommunications and Multimedia Applications (iTEAM), Universitat Politècnica de València (UPV), and the Department of Applied Physics Electromagnetism, Institute of Materials Science (ICMUV), Universitat de València (UVEG), Valencia. Since 2008, she has been a Technical Researcher with the iTEAM, UPV. Since 2010, she has been a Laboratory Engineer with European Space Agency (ESA), Val Space Consortium (VSC), Valencia. Her current research interest includes the analysis of the effects of high-power microwave devices.

Ana Vidal Pantaleoni (Member, IEEE) was born in Valencia, Spain, in 1970. She received the Ingeniería de Telecomunicaciones degree from the Universidad Politécnica de Valencia, Valencia, Spain, in 1993.

She stayed one year with the University of Strathclyde, Glasgow, U.K., under the Erasmus International Exchange Program. In 1993, she was involved in broadband communications development in the main research center of Telecom Portugal. She then became a Research Assistant with the Universidad Politécnica de Valencia. In 1995 and 1996, she held a Spanish trainee position with the European Space research and Technology Centre (ESTEC)–European Space Agency (ESA), Noordwijk, The Netherlands, where she was involved in the study and implementation of software for synthetic aperture radar (SAR) image processing. In 1996, she returned to the Universidad Politécnica de Valencia, where she held several lecturing positions, and became an Associate Professor in 2001. Her current interests are remote sensing data classification, GNSS algorithms, and numerical methods for microwave structures analysis, including high-power effects.

David Raboso received the Licenciado en Ciencias Físicas degree from the Autonomous University of Madrid, Madrid, Spain, in 1992, and the master's degree in space engineering from the University of Delft, Delft, The Netherlands, in 2002.

In 1992, he joined the European Space Agency, Noordwijk, The Netherlands, where he became responsible for all activities related to RF breakdown in space microwave components. He is a co-inventor of nine patents. He has coauthored more than 100 articles in prestigious journals.

Mariano Baquero-Escudero (Member, IEEE) was born in Murcia, Spain, on January 11, 1962. He received the Ingeniero de Telecomunicación degree from the Universidad Politécnica de Cataluña, Barcelona, Spain, in 1986, and the Ph.D. degree from the Universitat Politècnica de València (UPV), València, Spain, in 1994.

From 1986 to 1988, he was with the Antennas, Microwave and Radar Group, UPC, where he was involved with the development of a cylindrical nearfield facility to measure a 3-D radar antenna in CESELSA. Since 1989, he has been with the UPV, where he became a Full Professor in 2003. In 1995, he held a postdoctoral grant with the Joint Research Centre, European Commission, Ispra, Italy, where he developed high-resolution algorithms for radar applications. From April 1996 to February 1998, he was a Vice-Dean of the Telecommunications Engineering School of Valencia. He is currently with the Communications Department and the Institute of Telecommunications and Multimedia Application, Universitat Politècnica de València. His main research interests include microwave circuit and antenna analysis, design, and measurement.

Vicente E. Boria (Fellow, IEEE) was born in Valencia, Spain, in 1970. He received the Ingeniero de Telecomunicación degree (Hons.) and the Doctor Ingeniero de Telecomunicación degree from the Universidad Politécnica de Valencia, Valencia, Spain, in 1993 and 1997, respectively.

In 1993 he joined the Departamento de Comunicaciones, Universidad Politécnica de Valencia, where he has been Full Professor since 2003. In 1995 and 1996, he was holding a Spanish trainee position with the European Space Research and Technology Centre, European Space Agency (ESTEC-ESA), Noordwijk, The Netherlands, where he was involved in the area of EM analysis and design of passive waveguide devices. He has authored or coauthored 15 chapters in technical textbooks, 200 articles in refereed international technical journals, and over 250 articles in international conference proceedings. His current research interests are focused on the analysis and automated design of passive components (in particular filters and multiplexers), as well as on the simulation and measurement of power effects in high-frequency devices and systems.

Prof. Boria has been a member of the IEEE Microwave Theory and Techniques Society (IEEE MTT-S) and the IEEE Antennas and Propagation Society (IEEE AP-S) since 1992. He acts as a Regular Reviewer of the most relevant IEEE and IET Technical Journals on his areas of interest. He has been an Associate Editor of the IEEE MICROWAVE AND WIRELESS COMPONENTS LETTERS from 2013 to 2018 and *IET Electronics Letters* from 2015 to 2018. He serves as a Subject Editor (Microwaves) of *IET Electronics Letters* and as an Editorial Board member of *International Journal of RF and Microwave Computer-Aided Engineering*. He is also a member of the Technical Committees of the IEEE-MTT International Microwave Symposium and the European Microwave Conference.